Journal of Molecular Catalysis A: Chemical 290 (2008) 60–66

Contents lists available at ScienceDirect

Journal of Molecular Catalysis A: Chemical

journal homepage: www.elsevier.com/locate/molcata

Lewis acid metal ion-exchanged MAPO-36 molecular sieve: Characterisation and catalytic activity

S. Vishnu Priya, J. Herbert Mabel, S. Gopalakrishnan, M. Palanichamy, V. Murugesan*

Department of Chemistry, Anna University, Chennai 600025, India

ARTICLE INFO

Article history:
Received 21 February 2008
Received in revised form 2 May 2008
Accepted 6 May 2008
Available online 15 May 2008

Keywords:
Magnesium aluminophosphate
Ion-exchange
Acidity
tert-Butylation

ABSTRACT

Magnesium aluminophosphate-36 (MAPO-36) molecular sieve was synthesised hydrothermally and subjected to wet ion-exchange with Fe^{3+}, Zn^{2+}, La^{3+} or Ce^{3+}. They were characterised by using XRD, SEM, temperature programmed desorption (TPD) of ammonia and thermogravimetric analysis (TGA). The XRD patterns of ion-exchanged MAPO-36 exhibit similar features to that of MAPO-36, which revealed no structural degradation during ion-exchange. TPD (ammonia) showed selective ion-exchange of strong acid sites for Fe^{3+}, La^{3+} and Ce^{3+} but not for Zn^{2+}. Based on the results of TGA the actual species involved in the ion-exchange is suggested to be $M(OH)_2^+$, which upon calcination converted to MO^+ where M is Fe^{3+}, La^{3+} or Ce^{3+}. *tert*-Butylation of phenol was carried out in the vapour phase as a probe reaction to examine the catalytic activity of MAPO-36 and ion-exchanged MAPO-36 molecular sieves. The ion-exchanged catalysts were found to be more active than the parent MAPO-36 and also showed higher selectivity to 4-*tert*-butylphenol.

1. Introduction

Crystalline microporous aluminophosphate molecular sieves (AlPOs) continue to sustain research interest in the area of catalysis and adsorption [1,2]. Since the parent AlPOs are devoid of any acid sites, they are not suitable for catalysis. Hence incorporation of silicon in the place of framework phosphorous or divalent cations in the place of Al^{3+} becomes a prerequisite to generate catalytic activity [3,4]. Many metals containing AlPO molecular sieves have already been reported in the literature [5–11]. These metal-containing molecular sieves, particularly M^{2+} ions in the framework, carry net negative charge balanced by protons. Zahedi-Niaki et al. [12] were the first to report the synthesis of AlPO-36 with ATS structure type, free from any element other than Al, P and O. It possesses one-dimensional channels parallel to *c*-axis. The pore apertures are formed by 12 corner shared TO_4 (T = Al, P, etc.) tetrahedral units, resulting in an elliptical shape with a dimension of 7.4 × 6.5 Å. Since the parent material does not possess any Bronsted acidity, incorporation of M^{2+} (M = Mg) ions is indispensable in generating acidity for application in catalysis as reported by Meier et al. [13]. The presence of metal ions in the framework affects ion-exchange and metal specific behaviour of the material in addition to Bronsted acidity. MAPO-36 is of special interest in catalysis as it exhibits much higher catalytic activity than MAPO-5 and MAPO-11 particularly in cracking and disproportionation reactions in which Bronsted acid sites are the active sites [14]. Akolekar and Bhargava [15] reported wet ion-exchange of Na^+, Cs^+ and Ca^{2+} in MAPO-36 to catalyse isomerisation of *o*-xylene. But there is no report in the literature for ion-exchange of MAPO-36 with transition or rare earth metal ions. Beyer et al. [16] applied reductive solid-state ion-exchange method to introduce InO^+ ions into large pore NH_4NaY zeolite by replacing bridged protons. Mavrodinova et al. [17–20] also reported the introduction of InO^+ and AlO^+ ions into HY and Hβ zeolites. These reports revealed clearly that during ion-exchange with higher valent ions particularly trivalent ions, the actual ions used for ion-exchange are $M(OH)_2^+$ based on the Plank–Hirschler mechanism and it is converted to MO^+ during calcination. Considering these facts, the present study focused on the synthesis of MAPO-36 and its wet ion-exchange with transition and rare earth metal ions such as Fe^{3+}, Zn^{2+}, La^{3+} and Ce^{3+}. Their catalytic activity was evaluated in the *tert*-butylation of phenol in the vapour phase. This reaction was selected as a model reaction because of its industrial importance. Many alkylated phenols are used as raw materials for the production of resins, agrochemicals, antioxidants, UV absorbers and heat stabilizers for polymeric materials [21].

* Corresponding author. Tel.: +91 44 22203144; fax: +91 44 22200660/22350397.
E-mail address: v_murugu@hotmail.com (V. Murugesan).

1381-1169/$ – see front matter © 2008 Elsevier B.V. All rights reserved.
doi:10.1016/j.molcata.2008.05.005

2. Experimental

2.1. Preparation of catalysts

Hydrothermal synthesis of MAPO-36 was carried out with a slight modification of the procedure reported by Zahedi-Niaki et al. [22] using a gel composition of $1.83Pr_3N{:}0.92Al_2O_3{:}0.17MgO{:}1P_2O_5{:}80H_2O$. Aluminium isopropoxide (Merck), phosphoric acid (Merck) (88%), magnesium nitrate (Merck) and tripropylamine (Sigma–Aldrich) were used as sources for Al, P and Mg, respectively in the synthesis. Aluminium isopropoxide (5.5 g) was soaked in distilled water (10 mL) for 24 h and stirred vigorously using a mechanical stirrer for 1 h. Meanwhile phosphoric acid (11.5 g) and magnesium nitrate (4.4 g) were dissolved in distilled water (26 mL) and added to the above solution under stirring. The stirring was continued for 2 h. Then the template, tripropylamine (12.9 g) was added and the pH of resulting gel was found to be 9. The gel was autoclaved at 165 °C for 72 h. The crystallized product was separated from the mother liquor (pH 7) by filtration and dried at 80 °C for 12 h. The assynthesized material was calcined at 550 °C for 8 h to remove the template.

About 2 g of the calcined material was taken in a round bottom flask. The corresponding metal nitrate solution (30 mL; 0.05 M) was added into the flask. The solution was stirred under reflux condition for 12 h. The resulting suspension was decanted and the solid sample was dried at 80 °C for 6 h. The same procedure was repeated thrice. The solid sample was then washed thoroughly and repeatedly with distilled water to remove the excess metal nitrate. The sample was then dried and calcined at 600 °C for 6 h. These samples were used for characterisation and catalytic studies.

2.2. Physicochemical characterisation

The powder X-ray diffraction (XRD) patterns of samples were recorded in a PANalytical X'pert PRO diffractometer using nickel-filtered Cu Kα (0.154 nm) radiation and a liquid nitrogen-cooled germanium solid-state detector. The diffractograms were recorded in the 2θ range of 5–40° in steps of 1.2° with a count time of 10 s at each point. Thermogravimetric analysis (TGA) of the materials was performed using a high resolution PerkinElmer TG-DTA diamond series. The samples were heated under nitrogen atmosphere at a heating rate of 10 °C min^{-1} in the temperature range 50–750 °C. The morphology was observed using a scanning electron microscope (SEM) (Stereo Scan LEO 440). The acidity of calcined samples was determined by temperature programmed desorption (TPD) of ammonia using a Micromeritics Chemisorb 2750 pulse chemisorption system. Approximately 50 mg of the sample was placed in a U shaped, flow-through, quartz microreactor activated at 500 °C for 2 h with helium flow of 20 mL min^{-1}. The sample was cooled to 100 °C and then exposed to ammonia. The sample was again flushed with helium for half an hour to remove the physisorbed ammonia. Desorption profile was then recorded by increasing the sample temperature from 100 to 600 °C at a rate of 5 °C min^{-1}.

2.3. Catalytic performance

The reaction was carried out in a fixed-bed, vertical-flow-type reactor made up of borosil glass tube 40 cm in length and 2 cm in internal diameter. About 0.5 g of the sample was placed in the middle of the reactor and supported on either side with a thin layer of quartz wool and ceramic beads. The reactor was heated to the requisite temperature with the help of a tubular furnace controlled by a digital temperature controller cum indicator. Reactants were fed into the reactor using a syringe infusion pump (SAGE instrument) that could be operated at different flow rates. The reaction

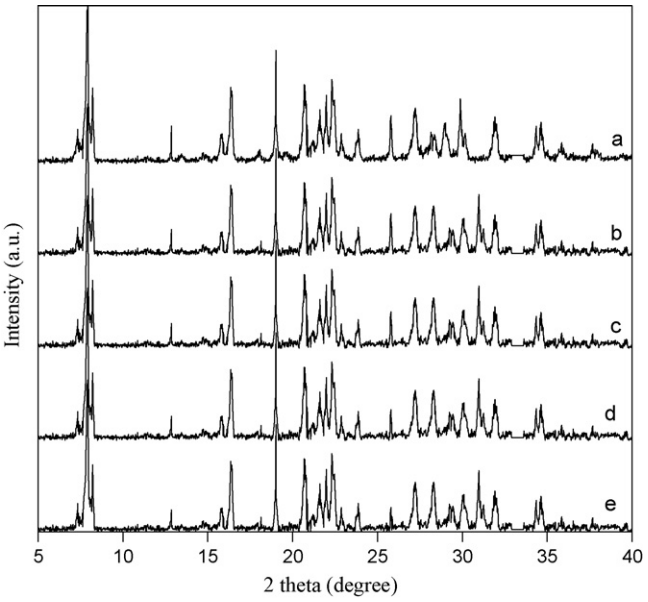

Fig. 1. XRD patterns of (a) MAPO-36, (b) FeMAPO-36, (c) ZnMAPO-36, (d) LaMAPO-36 and (e) CeMAPO-36.

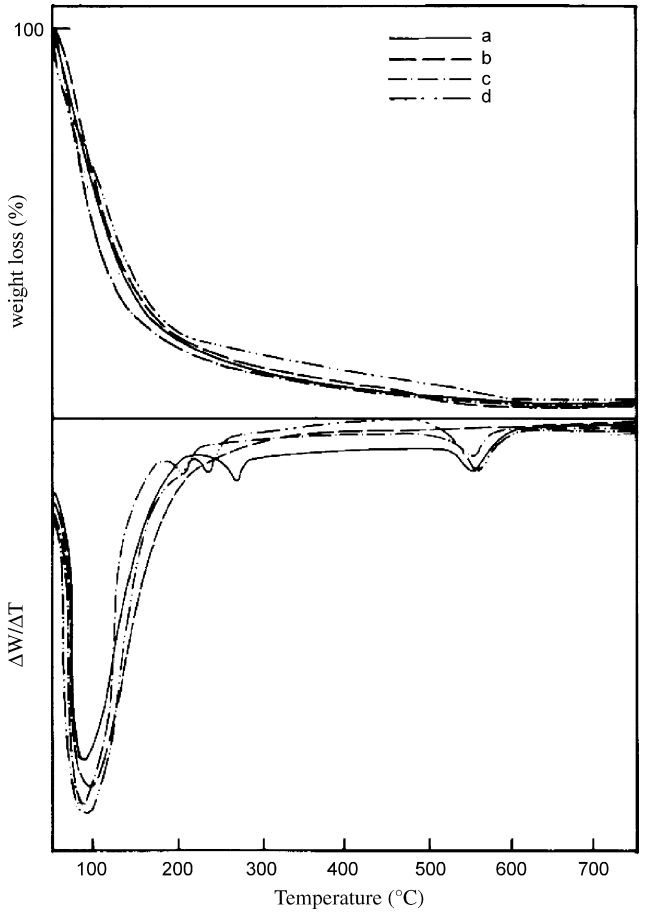

Fig. 2. TG/DTG curves of (a) FeMAPO-36, (b) ZnMAPO-36, (c) LaMAPO-36 and (d) CeMAPO-36.

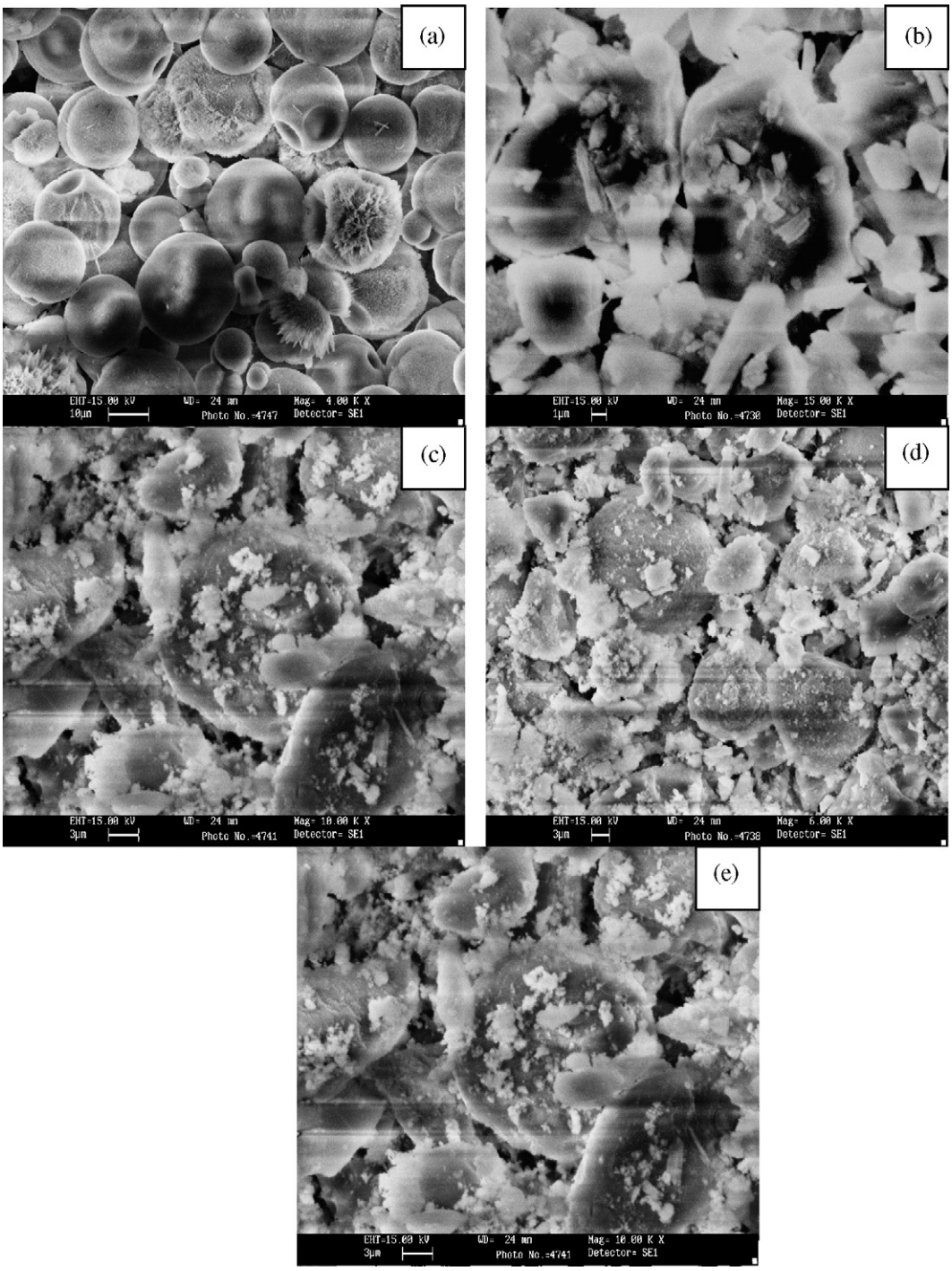

Fig. 3. SEM pictures of (a) MAPO-36, (b) FeMAPO-36, (c) ZnMAPO-36, (d) LaMAPO-36 and (e) CeMAPO-36.

was carried out at atmospheric pressure. The bottom of the reactor was connected to a coiled condenser and a receiver to collect the products. The products obtained in the first 10 min were discarded, and the product collected after 1 h was analysed for identification. The products were analysed by a Shimadzu 17A gas chromatograph (crosslinked 5% phenyl methyl siloxane capillary column, FID detector) and confirmed by a PerkinElmer Auto system XL gas chromatograph coupled with Turbo mass spectrometer using helium as carrier gas at a flow rate of 1 mL min^{-1}. After each catalytic run, the catalyst was regenerated by passing moisture and carbon-dioxide-free air through the reactor for 6 h at 500 °C.

3. Results and discussion

3.1. Characterisation

XRD powder diffraction patterns of calcined MAPO-36 and ion-exchanged MAPO-36 are shown in Fig. 1. The XRD patterns of MAPO-36 coincide with the one already reported in the literature [23]. The XRD patterns of ion-exchanged MAPO-36 molecular sieves also show similar features as that of MAPO-36 and hence there is no structural degradation during ion-exchange. Further, there are no patterns corresponding to non-framework metal oxide

in the XRD patterns of ion-exchanged MAPO-36 molecular sieves. Though the patterns appear almost similar for all samples, there is a very slight decrease in the intensity of peaks at 27 and 30° (2θ). In addition there is minimum peak broadening above 35° (2θ). But there are no distinct patterns corresponding to any of the metal oxides of metal ions used for ion-exchange. Hence the metal oxides even if present are in low amount below the detectable limit of XRD.

The TGA results of ion-exchanged MAPO-36 are illustrated in Fig. 2. DTG curves are also shown in the same figure. The thermogram of FeMAPO-36 (Fig. 2a) shows an initial weight loss below 150 °C due to desorption of water. The second minute weight loss between 200 and 400 °C is due to decomposition of $Fe(OH)_3$ formed during ion-exchange. But non-framework Fe_2O_3 is not detected in the XRD analysis. Hence it may be present in a trace amount and the grain size is not sufficient enough to be detected by XRD. The third weight loss between 500 and 600 °C is assigned to the decomposition of charge compensating $Fe(OH)_2^+$ to FeO^+ species. The existence of $Fe(OH)_2^+$ species is based on the Plank–Hirschler mechanism [24]. The thermograms of La and CeMAPO-36 (Fig. 2c and d) appear similar to that of FeMAPO-36. The presence of MO^+ (M = La^{3+} and Ce^{3+}) species in these molecular sieves is also evident. The thermogram of ZnMAPO-36 (Fig. 2b) differs from others and hence Zn^{2+} does not produce ZnO^+ species. In other words the Plank–Hirschler mechanism is not applicable to metal ions in +2 oxidation state. Fe^{3+}, La^{3+} and Ce^{3+} with their high ionic potential can readily undergo hydrolysis to form $M(OH)_2^+$ which then become MO^+ during calcination. The SEM pictures of calcined MAPO-36 and ion-exchanged MAPO-36 are shown in Fig. 3. The SEM picture of MAPO-36 shows spherical particles of various sizes. There are pits on the surface of particles and the presence of such pits in the SEM picture of MAPO-36 is already reported by Machado and Cardoso [25]. Careful examination of SEM picture indicates aggregation of fine needles in an organized way to provide spherical sponge like morphology of different sizes. The SEM picture of FeMAPO-36 (Fig. 3b) illustrates destruction of small amount of spherical morphologies into small particles in irregular shape. Each particle possesses the needle shape of different sizes. Since iron nitrate solution was used for ion-exchange, the pH of the medium may be low. This may lead to cleavage of bigger particles into smaller ones. The SEM picture of ZnMAPO-36 (Fig. 3c) also illustrates destruction of spherical particles into smaller ones but to a lesser degree than FeMAPO-36. Similar features are also evident in the SEM pictures of La and CeMAPO-36 (Fig. 3d and e).

TPD (ammonia) was carried out between 100 and 600 °C for calcined MAPO-36 and ion-exchanged MAPO-36 catalysts. The results are illustrated in Fig. 4. Desorption of ammonia up to 200 and above 500 °C indicates the presence of weak acid sites and strong Bronsted acid sites, respectively. Lewis acid metal ions, weak Bronsted acid sites and defective sites are included as weak acid sites. The volume of ammonia desorbed from weak and strong acid sites per gram of the catalyst and the maximum temperature corresponding to each desorption are shown in Table 1. The total number of acid sites was found to be 5.1×10^{-5} mol g^{-1}. As a result of ion-exchange decrease in the number of strong acid sites and increase in the number of weak acid sites are observed in FeMAPO-36. This clearly demonstrates that only a part of strong acid sites are ion-exchanged. The weakly acidic nature of La^{3+} ions has been reported already in La^{3+} ion-exchanged H-ZSM-5 [26]. In addition La^{3+} ions were not shown to reduce the effective pore volume of the catalyst or increase the steric hindrance for the passage of linear molecules through the pores of the catalyst [26]. When La^{3+} ions are ion-exchanged there will be loss of three protons in the framework. However, there may be splitting of co-ordinated water molecules around La^{3+} ions to form two protons and $La(OH)_2^+$. These two

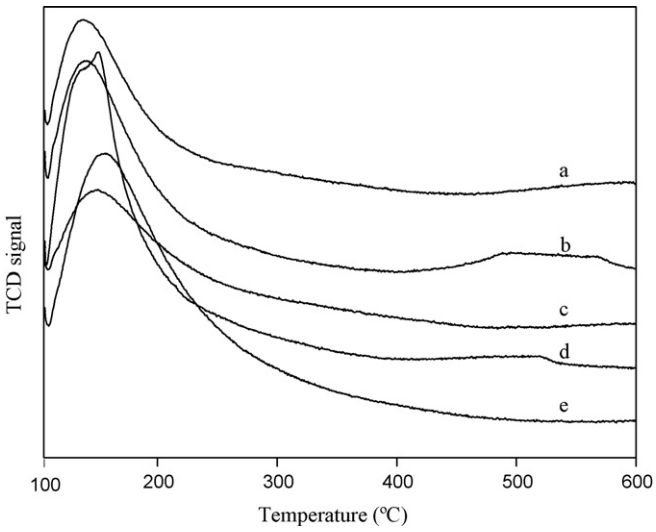

Fig. 4. Temperature programmed desorption (ammonia) of (a) MAPO-36, (b) FeMAPO-36, (c) ZnMAPO-36, (d) LaMAPO-36 and (e) CeMAPO-36.

newly formed protons will be taken up by two oxygen bridges of the framework. These two protons may not be as acidic as that of actually exchanged strongly acidic protons. This confirms that weak acid sites are generated as a result of ion-exchange. Thus the weak acid sites include weak Bronsted acid sites, Lewis acid sites and defective sites [24]. During calcination $La(OH)_2^+$ becomes LaO^+ as discussed already. More number of strong acid sites in ZnMAPO-36 are used for ion-exchange whereas only a part of them are ion-exchanged in FeMAPO-36. This demonstrates that the charge of a metal ion significantly influences the ion-exchange. The complete absence of strong acid sites in La and CeMAPO-36 is again an unusual and novel result. This kind of selective ion-exchange could be useful for some specific chemical transformations which require only weak acid sites provided LaO^+ and CeO^+ are not active in such reactions. In addition, selective transformations could also be made exclusively with MO^+ if weak Bronsted acid sites are not active in such reactions. As discussed in FeMAPO-36, there is also increase in the density of weak acid sites in both La and CeMAPO-36.

If the volume of ammonia corresponding to weak acid sites (0.94 mL g^{-1}) in MAPO-36 is subtracted from the volume of ammonia corresponding to that of LaMAPO-36 (2.26 mL g^{-1}), it is equal to 1.32 mL g^{-1}. Hence the total number of weak acid sites in LaMAPO-36 and CeMAPO-36 may also include Lewis acid metal ions in addition to weak Bronsted acid sites. Hence Fe^{3+}, La^{3+} and Ce^{3+} metal ions may not exist as M^{3+} during ion-exchange but as $M(OH)_2^+$ as predicted by the Plank–Hirschler mechanism. The same

Table 1
TPD (ammonia) results of MAPO-36 and ion-exchanged MAPO-36

Catalyst	Temperature (°C)	Volume (mL g^{-1} at STP)
MAPO-36	137	0.94
	592	0.20
FeMAPO-36	146	1.29
	545	0.12
ZnMAPO-36	146	0.93
	590	0.04
LaMAPO-36	162	2.26
	>500	–
CeMAPO-36	147	2.03
	>500	–

Table 2
Effect of temperature on phenol conversion and products selectivity

Temperature (°C)	Conversion (%)	Selectivity (%)			
		2-TBP	4-TBP	2,4-di-TBP	Others
200	32.7	30	47	17	6
250	44.3	24	54	14	8
300	50.2	13	69	9	9
350	47.0	12	65	7	16
400	40.5	9	58	6	27

Catalyst: CeMAPO-36; Feed ratio: 1:1 and WHSV: 2.80 h^{-1}.

may be converted to MO^+ during calcination as shown below.

$$M(H_2O)_6^{3+} \xrightarrow{\text{calcination}} MO^+ + 5H_2O + 2H^+$$

3.2. Catalytic performance

tert-Butylation of phenol with *tert*-butyl alcohol was investigated over calcined MAPO-36 and Fe, Zn, La and CeMAPO-36 in the vapour phase. The phenol conversion and products selectivity over CeMAPO-36 are presented in Table 2. The major products were found to be 2-*tert*-butylphenol (2-TBP), 4-*tert*-butylphenol (4-TBP) and 2,4-di-*tert*-butylphenol (2,4-di-TBP). The phenol conversion increases from 200 to 300 °C and then decreases. The decrease in the phenol conversion above 300 °C is due to coke formation. The formation of coke was confirmed physically. Such coke deposits were mainly due to the formation of polyalkylated phenolics and polybutenes [27]. Alkylation of phenol occurs through dissociative chemisorption of phenol on MO^+ and the resulting phenolic proton is transferred to its neighbouring bridging oxygen [28]. *tert*-Butyl alcohol is chemisorbed on the protonic sites to form *tert*-butyl cation which then undergoes electrophilic attack at the *o*- or *p*- position of the adjacent chemisorbed phenol yielding 2-TBP or 4-TBP (Scheme 1). This is the main route to the formation of 2-TBP and 4-TBP. Phenol can also be chemisorbed on the Bronsted acid sites of the catalyst and there may be *tert*-butyl cations close to it remaining as charge compensating cations. The reaction between them leads to the formation of 2-TBP and 4-TBP as shown in Scheme 2.

It is indirectly evident that the formation of 4-TBP may occur by the reaction between free phenol in the vapour phase and chemisorbed *tert*-butyl cation. Mathew et al. [29] also reported the formation of 4-TBP and 2,4-di-TBP due to the attack of phenol by *tert*-butyl cation in the adsorbed state as well as in the gaseous state. At lower temperatures phenol as well as alcohol may be clustering around the protonic sites which leads to slow electrophilic reaction. The clusters are lost gradually with increase in temperature, thus favouring enhanced free phenol concentration for electrophilic attack at the *p*-position. Although the *o*-position of phenol is not sterically crowded for electrophilic reaction, substitution at the *o*-position is slightly less due to repulsion between the positive charge on the *tert*-butyl cation and the positive charge of phenolic oxygen (Scheme 3).

Although the selectivity to 4-TBP was expected to increase with increase in temperature, decrease in the selectivity was observed at 350 and 400 °C. The decrease in the selectivity at higher tem-

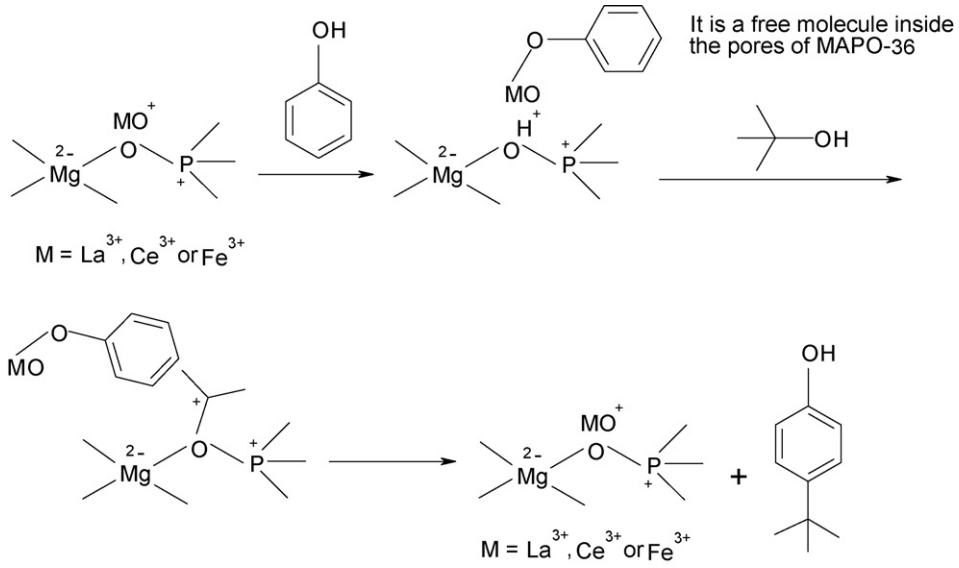

Scheme 1. *tert*-Butylation of phenol catalysed by MO^+.

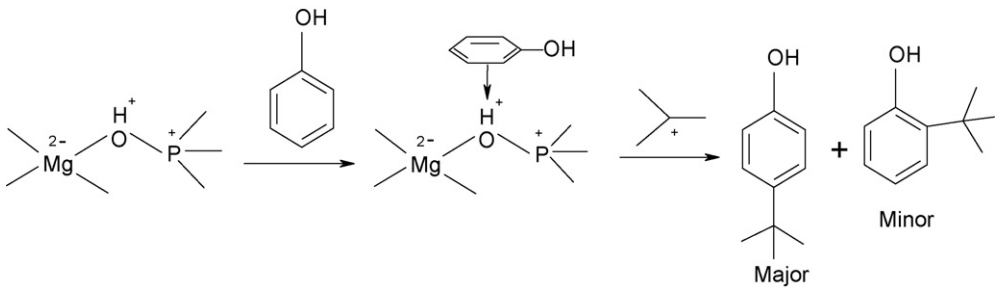

Scheme 2. *tert*-Butylation of phenol catalysed by Bronsted acid sites.

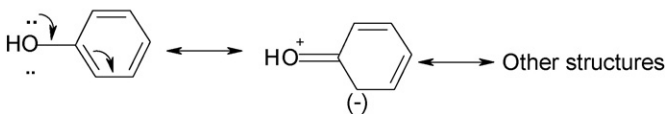

Scheme 3. Resonance structures in phenol.

peratures is largely due to its conversion to other products. The selectivity to 2,4-di-TBP also decreases with increase in temperature. This is also due to its conversion to other products, mainly polyalkylated phenolics. 2,4-di-TBP may be formed by the reaction between chemisorbed phenol and closely adsorbed *tert*-butyl cations. The above results therefore demonstrate the formation of 4-TBP with high selectivity. Kurian and Sugunan [30] and Huang et al. [31] have reported requirement of strong acid sites for the formation of 2,4-di-TBP in the alkylation of phenol with *tert*-butyl alcohol. However, di-alkylation depends only on the availability of *tert*-butyl cation for the monoalkylated products. Hence even with weak acid sites di-alkylated products could be formed. Even after coke formation, the pores are large enough to form other products with high selectivity at high temperatures.

The same reaction was also studied over calcined MAPO-36 and Fe, Zn and LaMAPO-36 catalysts. The results are presented in Table 3. MAPO-36 is found to be the least active among the catalysts. This observation clearly establishes that the reaction is largely controlled by Lewis acid sites. Further, chemisorption of phenol on the Lewis acid sites appears to be more favourable than on the Bronsted acid sites. Among the ion-exchanged MAPO-36, CeMAPO-36 is the most active. Since CeO^+ sites are more active than LaO^+ sites, the former is considered to assist dissociative adsorption of phenol better. Ce^{3+} (0.102 nm) is smaller in size than La^{3+} (0.12 nm) due to lanthanide contraction is suggested to be the cause for its higher Lewis acidity. The selectivity to 4-TBP is higher than other products over all the catalysts. But Fe, La and CeMAPO-36 showed higher 4-TBP selectivity than ZnMAPO-36. The presence of both strong and weak acid sites in ZnMAPO-36 is the cause for the reduced selectivity to 4-TBP. Hence, Fe, La and CeMAPO-36 with more number of weak acid sites could be considered as better catalysts than others.

The reaction was also performed with feed ratios 1:2 and 1:3 over CeMAPO-36 at 300 °C and the results are shown in Table 4. The conversion was found to be high at 1:2 than other feed ratios. The less conversion with 1:3 is due to suppression of chemisorption of phenol in the presence of excess *tert*-butyl alcohol. Such

Table 3
Effect of catalyst on phenol conversion and products selectivity

Catalyst	Conversion (%)	Selectivity (%)			
		2-TBP	4-TBP	2,4-di-TBP	Others
MAPO-36	25.0	23	52	13	12
FeMAPO-36	33.0	18	60	12	10
ZnMAPO-36	28.2	24	56	12	8
LaMAPO-36	38.5	15	62	14	9
CeMAPO-36	50.2	13	69	9	9

Temperature: 300 °C; feed ratio: 1:1; and WHSV: 2.80 h^{-1}.

Table 4
Effect of feed ratio on phenol conversion and products selectivity

Phenol:*tert*-butyl alcohol	Conversion (%)	Selectivity (%)			
		2-TBP	4-TBP	2,4-di-TBP	Others
1:1	50.2	13	69	9	9
1:2	59.8	8	92	0	0
1:3	32.7	11	73	7	9

Catalyst: CeMAPO-36; catalytic temperature: 300 °C.

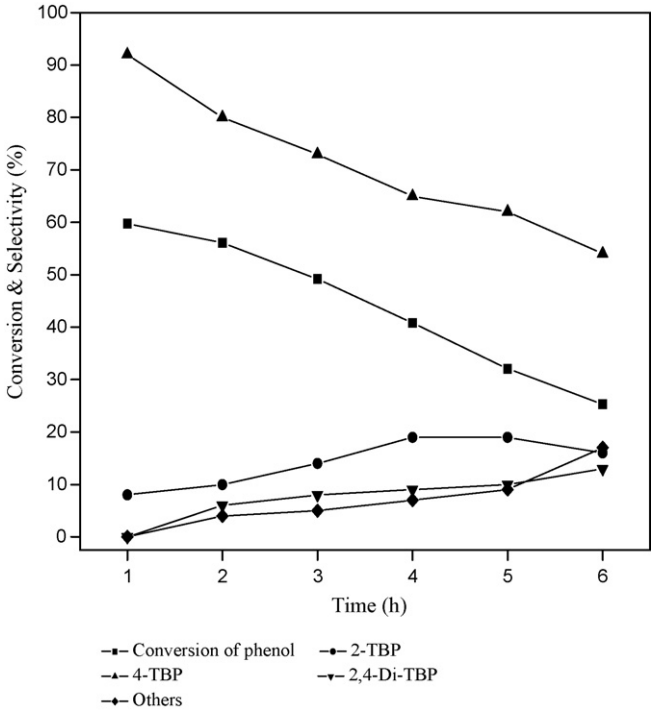

Fig. 5. Effect of time on stream on phenol conversion and products selectivity over CeMAPO-36.

observation has already been reported in the literature [32]. In addition, selectivity to 2-TBP, 2,4-di-TBP and others are suppressed to a larger extent. This suggests that polyalkylated products could be avoided by using the feed containing less amount of *tert*-butyl alcohol. The effect of dilution of phenol may also exist even with the feed ratio 1:2. But there are enough *tert*-butyl cations on the Bronsted acid sites which can attack free phenol thus yielding 4-TBP as the major product. The formation of 2-TBP and 2,4-di-TBP is due to chemisorption of phenol on Lewis acid sites. Phenol may be preferentially chemisorbed with 1:1 feed ratio which will enhance the selectivity of 2-TBP, 2,4-di-TBP and others. The less selectivity to 4-TBP also supports this view. This study concludes that phenol can be selectively alkylated at the *p*-position with 1:2 feed ratio.

The effect of WHSV on phenol conversion and products selectivity was studied over CeMAPO-36 with a feed ratio 1:2. The conversion decreases with increase in WHSV due to rapid diffusion of reactants. The selectivity to 2-TBP decreases while that to 4-TBP slightly increases with increase in WHSV, thus supporting the hypothesis that selective formation of 4-TBP requires reaction between free phenol and *tert*-butyl cation on the catalyst surface.

The effect of time on stream was studied for 6 h over CeMAPO-36 at 300 °C with the 1:2 feed ratio and WHSV 2.81 h^{-1} and the results are shown in Fig. 5. The conversion decreases gradually with increase in time on stream and at the end of 6 h stream only 25% conversion is observed. The selectivity to 2-TBP increases up to 4 h, remains steady between 4th and 5th h and decreases there after, whereas the selectivity to 4-TBP decreases rapidly in the initial period of time on stream. This is due to enhanced initial activity on the Lewis acid sites, followed by deactivation at the expense of rapid process of accumulation of reaction products and intermediates [20]. Thus the deactivation of the catalyst at longer hours of time on stream may be due to accumulation of reaction products on the active sites and blocking of Lewis acid sites by coke. 2,4-di-TBP selectivity increases with increase in time on stream due to conversion of mono alkylated products to 2,4-di-TBP.

4. Conclusion

This study revealed that Bronsted acid sites of MAPO-36 could be ion-exchanged with Lewis acid metal ions such as Zn^{2+}, Fe^{3+}, La^{3+} and Ce^{3+} by wet ion-exchange. The ion-exchange does not affect the structural integrity of the parent MAPO-36. The selective and complete ion-exchange of strong acid sites in LaMAPO-36 and CeMAPO-36 is an interesting observation in this investigation. Based on the Plank–Hirschler mechanism it is concluded that the actual species of ion-exchange is $M(OH)_2^+$ which decomposes to form MO^+ during calcination. The other important observation of this study is 90% selectivity of 4-TBP. Hence it is concluded that Lewis acid ion-exchanged MAPO-36 could find significant use as catalyst in the selective alkylation of phenolics.

Acknowledgements

The authors gratefully acknowledge the financial support from the Department of Science and Technology (DST) (Sanction No. SR/S1/PC-24/2003), Government of India, New Delhi, for this research work. One of the authors (S. Vishnu Priya) is grateful to DST for the award of Senior Research Fellowship (SRF). The authors like to place on record the financial supports from University Grants Commission (UGC) under Special Assistance Programme (DRS) and DST under FIST Programme for the sophisticated equipments facilities in the Department.

References

[1] J.A. Rabo, in: J.A. Rabo (Ed.), Zeolite Chemistry and Catalysis, ACS Monograph, 171, American Chemical Society, Washington, DC, 1976, p. 332.
[2] A.V. Kucherov, A.A. Slinkin, Zeolites 6 (1986) 175.
[3] B.M. Lok, C.A. Messina, R.L. Patton, R.T. Gajek, T.R. Cannan, E.M. Flanigen, US Patent 4,440,871 (1984).
[4] B.M. Lok, C.A. Messina, R.L. Patton, R.T. Gajek, T.R. Cannan, E.M. Flanigen, J. Am. Chem. Soc. 106 (1984) 6092.
[5] C.A. Messina, B.M. Lok, E.M. Flanigen, US Patent 4,544,143 (1985).
[6] S.T. Wilson, E.M. Flanigen, Eur. Pat. Appl. 132 (1985) 708.
[7] S.T. Wilson, E.M. Flanigen, US Patent 4,567,029 (1986).
[8] S.P. Elangovan, B. Arabindoo, V. Krishnasamy, V. Murugesan, J. Chem. Soc., Faraday Trans. 91 (1995) 4471.
[9] D.B. Akolekar, Appl. Catal. A: Gen. 112 (1994) 125.
[10] C. Kannan, S.P. Elangovan, M. Palanichamy, V. Murugesan, Indian J. Chem. Technol. 5 (1998) 65.
[11] V. Umamaheswari, C. Kannan, B. Arabindoo, M. Palanichamy, V. Murugesan, Proc. Indian Acad. Sci. 112 (2000) 439.
[12] M.H. Zahedi-Niaki, P.N. Joshi, S. Kaliaguine, Chem. Commun. (1996) 47.
[13] W.M. Meier, D.H. Olson, Ch. Baerlocher, Atlas of Zeolites Structure Types, 4th ed., Elsevier, London, 1996, p. 1.
[14] E.M. Flanigen, R.L. Patton, S.T. Wilson, Stud. Surf. Sci. Catal. 37 (1988) 13.
[15] D.B. Akolekar, S. Bhargava, J. Mol. Catal. A: Chem. 122 (1997) 81.
[16] H.K. Beyer, R.M. Mihályi, C.H. Minchev, Y. Neinska, V. Kanazirev, Micropor. Mater. 7 (1996) 333.
[17] V. Mavrodinova, M. Popova, Y. Neinska, Ch. Minchev, Appl. Catal. A: Gen. 210 (2001) 397.
[18] V. Mavrodinova, M. Popova, R.M. Mihályi, G. Pál-Borbély, Ch. Minchev, Appl. Catal. A: Gen. 248 (2003) 197.
[19] V. Mavrodinova, M. Popova, R.M. Mihályi, G. Pál-Borbély, Ch. Minchev, Appl. Catal. A: Gen. 262 (2004) 75.
[20] V. Mavrodinova, M. Popova, R.M. Mihályi, G. Pál-Borbély, Ch. Minchev, J. Mol. Catal. A: Chem. 220 (2004) 239.
[21] H. Fiege, H.-W. Voges, in: B. Elvera, S. Hawkins, M. Ravenscroft, G. Schulz (Eds.), Phenol Derivatives: In Ullmann's Encyclopedia of Industrial Chemistry, A19, fifth ed., VCH Publications, Germany, 1989, p. 313.
[22] M.H. Zahedi-Niaki, P.N. Joshi, S. Kaliaguine, Chem. Commun. (1996) 1373.
[23] J.V. Smith, J.J. Pluth, K.J. Andries, Zeolites 13 (1993) 166.
[24] P. Tynjala, T.T. Pakkanen, J. Mol. Catal. A: Chem. 110 (1996) 153.
[25] M.S. Machado, D. Cardoso, Chem. Mater. 11 (1999) 3238.
[26] R.W. Hartford, M. Kojima, C.T. O'Connor, Ind. Eng. Chem. Res. 28 (1989) 1748.
[27] Z. Liu, P. Moreau, F. Fajula, Appl. Catal. A: Gen. 159 (1997) 305.
[28] K. Shanmugapriya, S. Saravanamurugan, M. Palanichamy, B. Arabindoo, V. Murugesan, J. Mol. Catal. A: Chem. 223 (2004) 177.
[29] T. Mathew, B.S. Rao, C.S. Gopinath, J. Catal. 222 (2004) 107.
[30] M. Kurian, S. Sugunan, Catal. Commun. 7 (2006) 417.
[31] J. Huang, L. Xing, H. Wang, G. Li, S. Wu, T. Wu, Q. Kana, J. Mol. Catal. A: Chem. 259 (2006) 84.
[32] A. Corma, V. Fornes, M.T. Navarro, J. Perezpariente, J. Catal. 148 (1994) 569.